ARTICLES
https://doi.org/10.1038/s41929-022-00746-x

nature catalysis

Check for updates

OPEN

A cell-free self-replenishing CO_2-fixing system

Shanshan Luo[1,4], Paul P. Lin[2,4], Liang-Yu Nieh[2], Guan-Bo Liao[2], Po-Wen Tang[3], Chi Chen[3] and James C. Liao[2]✉

Biological CO_2 fixation is so far the most effective means for CO_2 reduction at scale and accounts for most of the CO_2 fixed on Earth. Through this process, carbon is fixed in cellular components and biomass during organismal growth. To uncouple CO_2 fixation from growth and cellular regulation, cell-free CO_2 fixation systems represent an alternative approach since the rate can be independently manipulated. Here we designed an oxygen-insensitive, self-replenishing CO_2 fixation system with opto-sensing. The system comprises a synthetic reductive glyoxylate and pyruvate synthesis (rGPS) cycle and the malyl-CoA-glycerate (MCG) pathway to produce acetyl-coenzyme A (CoA), pyruvate and malate from CO_2, which are also intermediates in the cycle. We solved various problems associated with the in vitro system, and implemented opto-sensing modules to control the regeneration of cofactors. We accomplished sustained operation for 6 hours with a CO_2-fixing rate comparable to or greater than typical CO_2 fixation rates of photosynthetic or lithoautotrophic organisms.

The annual anthropogenic CO_2 emission reached 40 $GtCO_2$ per year in 2019, with cumulative CO_2 emission exceeding 2,000 Gt (ref. [1]). To achieve net zero carbon emission by 2050 (ref. [2]), developing technologies for carbon fixation, storage and use have become an urgent issue. Until now, biology is the only demonstrated approach at scale capable of fixing and using CO_2 to produce a large variety of compounds. However, biological CO_2 fixation rate is controlled by cellular regulation that balances CO_2 fixation with cell physiology and organismal growth, and typically limited by oxygen sensitivity and the carboxylase activity. To decouple CO_2 fixation from cellular physiology and growth, in vitro cell-free enzymatic systems have been proposed, since the rate is in principle scalable with enzyme concentrations up to physicochemical limitations. However, in vitro systems need to overcome a few challenges, including enzyme instability, metabolite instability and cofactor regeneration.

Although various approaches have been reported to improve enzyme stability[3,4], metabolite stability[5,6] and cofactor recycling[7], these potential solutions cannot be simply applied to every case. Additionally, the lack of cellular regulation for in vitro cell-free systems also presents a problem in balancing the rates of cofactor consumption and regeneration under dynamic conditions. These problems need to be addressed to assess the feasibility of in vitro CO_2 fixation at scale. To overcome all these difficulties, we aim to construct a cell-free in vitro CO_2 fixation system with real-time opto-sensing modules to control the regeneration of cofactors. We first have to design a CO_2-fixing cycle in which each enzyme exhibits a high specific activity, and is readily purifiable and oxygen tolerant. Additionally, the cycle intermediates must self-replenish to allow for sustained drawing from any intermediate to the desirable product. We noted that except for the Wood–Lindahl pathway[8,9] and the reductive glycine pathway[10], all of natural CO_2-fixing pathways either individually or after coupling with other common pathways are self-replenishing cycles[11] (Supplementary Fig. 1), in which the product is also one of the intermediates. There are at least two advantages in this configuration. First, the self-replenishing cycle can operate in many ways, such that any intermediate can be withdrawn as a product. For example, the Calvin–Benson–Bassham (CBB) cycle can output C_3, C_4, C_5, C_6 or C_7 as a product, and still maintain a steady state, provided that the product was not drained beyond the rate of replenishing. This requirement is relatively easy to achieve by controlling the output activity. Second, the self-replenishing cycle accumulates products in the intermediates and can be autocatalytic[8,12]. This is helpful in the cycle startup phase when the concentrations of intermediates are below the K_M values and the accumulation of intermediates increases the rate of cycle.

Unfortunately, the naturally evolved CO_2-fixing cycles all contain key enzymes with intrinsic problems hindering further engineering (Supplementary Tables 1 and 2)[13]. For example, ribulose-1,5-bisphosphate carboxylase/oxygenase (RuBisCO), the key enzyme of the CBB cycle, has a relatively low velocity and has a notable oxygenase activity that leads to photorespiration[14]. Pyruvate-ferredoxin oxidoreductase (PFOR), one of the key enzymes in the Wood–Lindahl pathway, reductive tricarboxylic acid (rTCA) cycle, dicarboxylate/4-hydroxybutyrate (DC/4HB) cycle and the reductive glycine pathway[10], is oxygen sensitive and requires ferredoxin as the electron carrier[15]. These characteristics cause major difficulties when the enzyme is used under ambient conditions.

Here, we show the successful design and operation of an oxygen-insensitive, self-replenishing CO_2 fixation system with opto-sensing. The system comprises a synthetic reductive glyoxylate and pyruvate synthesis (rGPS) cycle and the MCG pathway. The self-replenishing feature allows every intermediate of rGPS–MCG cycle to be produced from CO_2 (Fig. 1 and Supplementary Fig. 4) and output as a product if the rate of product draining does not exceed the rate of replenishing. The opto-sensing system allows us to monitor and maintain the concentration of each cofactor (that is, [NAD(P)H], [ATP] and [FAD]). We accomplished sustained operation for 6 hours with a CO_2-fixing rate comparable to or greater than typical CO_2 fixation rates of photosynthetic or lithoautotrophic organisms.

Results

Design of the rGPS–MCG cycle. To design a highly efficient, oxygen-insensitive and self-replenishing CO_2-fixing cycle, we used a modular approach. We started from the oxygen-insensitive carboxylase, phosphoenolpyruvate (PEP) carboxylase (Ppc), which catalyses the carboxylation of PEP (C_3) to form the C_4 compound

[1]Department of Chemical and Biomolecular Engineering, University of California, Los Angeles, CA, USA. [2]Institute of Biological Chemistry, Academia Sinica, Taipei, Taiwan. [3]Research Center for Applied Sciences, Academia Sinica, Taipei, Taiwan. [4]These authors contributed equally: Shanshan Luo, Paul P. Lin. ✉e-mail: liaoj@gate.sinica.edu.tw

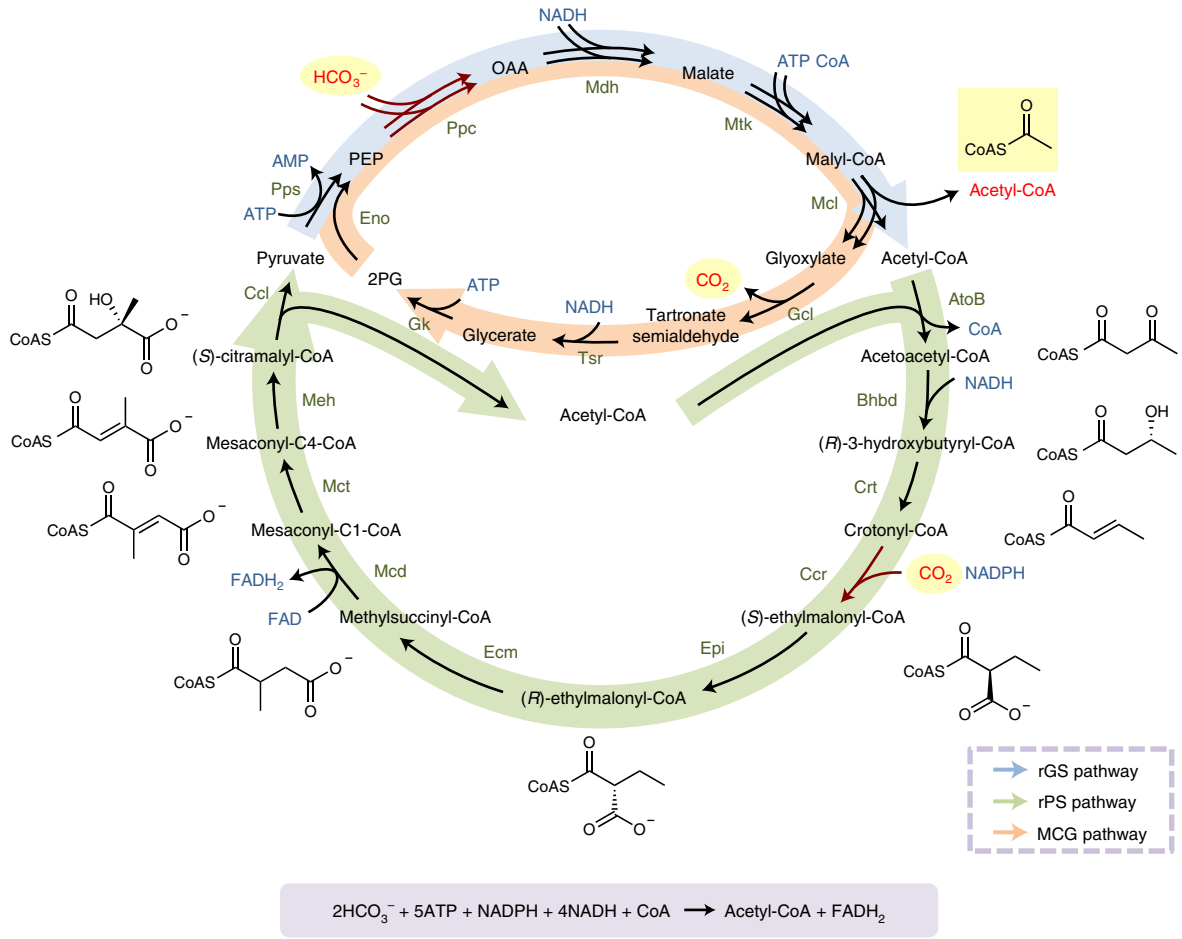

Fig. 1 | The rGPS–MCG cycle with acetyl-CoA as the end product. The rGPS cycle consists of the rGS pathway (blue) and the rPS pathway (green). The MCG pathway (orange) consists of the rGS pathway and the glycerate pathway. The red arrow indicates the carboxylation reaction. See Supplementary Table 3 for enzyme abbreviations of the rGPS cycle. Gcl, glyoxylate carboligase; Tsr, tartronate semialdehyde reductase; Gk, glycerate 2-kinase; Eno, enolase and 2PG, 2-phospho-D-glycerate.

oxaloacetate (OAA)[16]. It is one of the most active carboxylases with superior affinity toward HCO_3^- and has no oxygenase activity[17]. Ppc is used to replenish intermediates of the tricarboxylic acid cycle, or to shuttle CO_2 in C_4 or in the crassulacean acid metabolism in plants. However, in most cells, OAA cannot be converted to pyruvate or acetyl-CoA, without carbon loss. To overcome this limitation, we have previously designed and demonstrated a Ppc-based pathway to convert one C_3 compound (pyruvate) to two C_2 metabolites, acetyl-CoA and glyoxylate, with one bicarbonate fixed[18]. We termed this pathway the reductive glyoxylate synthesis (rGS) pathway (Fig. 1) and it contains part of the reverse glyoxylate shunt[18]. Then, in our follow-up work, we designed the MCG pathway[19], which consists of the rGS pathway and the glycerate pathway, to convert glyoxylate back to acetyl-CoA via glycerate (Supplementary Fig. 2d), with a net reaction of fixing one carbon to pyruvate to produce two acetyl-CoA (Supplementary Fig. 3).

To complete a CO_2 fixation cycle, another carboxylation reaction is needed to convert the C_2 product back to the C_3 compound, pyruvate. In nature, PFOR can fix one CO_2 to acetyl-CoA to produce pyruvate using reduced ferredoxin as the redox cofactor. However, the oxygen sensitivity of PFOR is a major challenge that precludes its function in aerobic organisms. Natural acetyl-CoA assimilation pathways could not fulfil this task either. For example, the glyoxylate cycle can only convert two acetyl-CoA to one pyruvate with one carbon loss. The ethylmalonyl-CoA pathway can convert two acetyl-CoA to one glyoxylate and one propionyl-CoA in nine steps. Theoretically, propionyl-CoA can be converted to pyruvate through the methylcitrate cycle in seven steps. However, the malate to OAA step in the methylcitrate cycle is needed in the reverse direction in the rGS pathway. This route could be challenging to implement with the rGS pathway for the complicated reaction network. Synthetic routes based on acetyl-CoA carboxylase or methylmalonyl-CoA carboxytransferase have been proposed to convert acetyl-CoA to pyruvate by Bar-Even et al.[17]. However, these pathways contain an oxygen-sensitive enzyme lactoyl-CoA dehydratase or alanine 2,3-aminomutase.

To design an oxygen-tolerant pathway that is functionally equivalent to PFOR for converting C_2 back to C_3, we used crotonyl-CoA carboxylase/reductase (Ccr), which catalyses the reductive carboxylation of crotonyl-CoA to (*S*)-ethylmalonyl-CoA using reduced nicotinamide adenine dinucleotide phosphate (NADPH) as the reducing equivalent[20]. This enzyme is the core carboxylase in the previously reported synthetic CO_2 fixation cycle, the crotonyl-CoA–ethylmalonyl-CoA–hydroxybutyryl-CoA (CETCH) cycle[21]. Similar to Ppc, Ccr catalyses the carboxylation reaction with a superior activity (Supplementary Table 1), and is oxygen insensitive. We designed a reductive pyruvate synthesis (rPS) pathway (Fig. 1) that first converts two acetyl-CoA to the C_5 intermediate mesaconyl-C1-CoA

with a CO_2 fixed, and then splits the C_5 compound to acetyl-CoA and pyruvate[22]. All ten enzymes involved are efficient and oxygen insensitive, thus avoiding all the challenges involved in PFOR. While this paper was under review, the rPS pathway was revealed by a computational approach[23] without experimental proof.

The reductive carboxylation of acetyl-CoA to pyruvate is thermodynamically unfavourable with a standard reduction potential ($E°'$) as low as −500 mV. Thus, using NADH ($E°' = -320$ mV, $E' = -280$ mV) or NADPH ($E°' = -320$ mV, $E' = -380$ mV) alone could not provide enough reducing power to push the reaction forward[24]. The rPS pathway realizes this reaction with one NADH and one NADPH and recovers excess reduction potential by producing one enzyme-bound $FADH_2$ ($E°' = -26$ mV)[25], thus rendering the reaction thermodynamically favourable. This approach is reminiscent of the naturally evolved bifurcating enzyme[26].

The rPS pathway converts one acetyl-CoA to pyruvate with one CO_2 fixed, and the rGS pathway converts one pyruvate to glyoxylate and acetyl-CoA while fixing one bicarbonate. Together, we obtained a CO_2 fixation cycle that produces glyoxylate. We call this CO_2 fixation pathway the reductive glyoxylate–pyruvate synthesis (rGPS) cycle. This rGPS cycle has been proposed as the CCR–PEPC pathway previously in silico[17] but never been demonstrated experimentally. Combining the rGPS cycle with the MCG pathway (or CCR–PEPC pathway with the glycerate pathway as suggested previously[17]), yields a self-replenishing CO_2 fixation cycle. Like the CBB cycle that can output C_3, C_4, C_5, C_6 or C_7 as a product, the rGPS–MCG cycle can output C_2, C_3, C_4 and C_5 (Fig. 1 and Supplementary Fig. 4), provided that the rate of product draining does not exceed the rate of replenishing. We applied maximum–minimum driving force analysis[27] to evaluate the thermodynamic feasibility of the rGPS–MCG cycle. The change in Gibbs energy of the reactions was estimated using the component contribution method[28]. Supplementary Fig. 5 indicates that each step is thermodynamically feasible (negative $\Delta_r G'^m$), except the acetyl-CoA acetyltransferase (AtoB) and crotonase (Crt) step, which can be driven by higher concentrations of the substrates. Such reactions have been shown multiple times in 1-butanol production[29].

Demonstration of the rGPS cycle. To demonstrate the feasibility of this synthetic network, we selected, cloned, expressed and purified 16 enzymes fused with His-tag in the rGPS–MCG cycle (Supplementary Fig. 6). The remaining three, Ppc, malate dehydrogenase (Mdh) and enolase (Eno), were acquired commercially. We have demonstrated the MCG pathway in vitro previously[19]. In this project, we further explored using pyruvate carboxylase (Pyc) to replace Pps and Ppc to convert pyruvate to OAA in the MCG pathway with lower ATP cost. We tried a commercial Pyc from Sigma. Although the commercial Ppc and Pyc have similar activities ($\geq$5 U mg^{-1}) according to the product information, we found using Pps and Ppc together achieved higher reaction rate of converting pyruvate to OAA than using Pyc. Pyc from *Corynebacterium glutamicum* has been expressed in *Escherichia coli* and purified successfully before, which could be another option. However, Pyc from *C. glutamicum* has a relatively high K_M (3.76 mM)[30] for pyruvate compared to *E. coli* Pps ($K_M = 83$ μM for pyruvate)[31] and Ppc ($K_M = 190$ μM for PEP)[32]. Although Pyc and Ppc have similar specific activities, Pps and Ppc couple could work better in our experimental condition probably due to the lower K_M values. Since Pps and Ppc couple worked well in our system, we did not explore more Pyc variants. Theoretically, using a Pyc with better kinetic parameters could improve rGPS–MCG cycle with lower ATP demand. The rest of the enzymes in the rGPS cycle were assayed for its activity either individually (Supplementary Fig. 7 and Supplementary Table 3) or sequentially (Supplementary Fig. 8).

After confirming the activity of each enzyme in the rGPS cycle, we set out to demonstrate the feasibility of the whole rGPS cycle. First, the rGPS cycle was divided into two segments on the basis of cofactor requirement. The first segment was from Pps to Ccr, which required ATP, NADH and NADPH as cofactors. The second segment was from ethylmalonyl-CoA/methylmalonyl-CoA epimerase (Epi) to (*S*)-citramalyl-CoA lyase (Ccl), which only required FAD as cofactor. Each segment was able to accomplish its desired activity (Supplementary Fig. 9a,b). We then demonstrated one round of the complete cycle in three steps in a one-pot reaction (Supplementary Fig. 9c,d). To operate the cycle continuously, FAD on (2*S*)-methylsuccinyl-CoA dehydrogenase (Mcd) must be regenerated from $FADH_2$. Mcd has been engineered to methylsuccinyl-CoA oxidase (Mco)[21], which can use O_2 as electron acceptor. Mco converts methylsuccinyl-CoA and O_2 to mesaconyl-CoA and H_2O_2. Then H_2O_2 can be converted back to O_2 through catalase. However, the V_{max} of Mco was 60 times lower than Mcd. Thus, we chose to still use Mcd in our system and tried to regenerate its cofactor, FAD. In the cell-free system, we used ferrocenium (Fc^+) as an artificial electron acceptor for FAD regeneration. Then ferrocene (Fc) can be oxidized back to Fc^+ using electrochemical approach (Supplementary Fig. 10c) or using horseradish peroxidase (Hrp) and H_2O_2 (Fig. 2 and Supplementary Fig. 10d), which can be generated renewably. We found that the CO_2 fixation rate is faster with Hrp than the electrochemical approach. Also, the Pt electrode from the electrochemical approach seems to adsorb free CoA and CoA-derived products. The binding between noble metal and thiol has been studied and reported in the literature[33]. Therefore, we continued with using Hrp to regenerate FAD in our following experiments, even though the electrochemical approach could still be a direction for future work. We optimized the working concentration range of ferrocenium (Supplementary Fig. 11a) to avoid the spontaneous reduction of Fc^+ by NAD(P)H and to ensure that Fc^+ can effectively work with Mcd (Supplementary Fig. 11b). The resulting working concentration of Fc^+ was set between 0 and 0.06 mM, and NAD(P)H concentration between 0.3 and 0.4 mM. Although Hrp can also oxidize NADH and NADPH with H_2O_2, the activity is more than 1,000 times lower than its activity with Fc^+ (Supplementary Fig. 12). By controlling the peroxidase amount in our system, Fc^+ can be regenerated with Hrp and H_2O_2 while NAD(P)H is barely influenced (Supplementary Fig. 13). To avoid enzyme damage, H_2O_2 was fed to the system manually (before the FAD/Fc^+ sensing and control module was implemented) on the basis of the decrease of Fc^+ concentration monitored by the absorbance at 300 nm. We demonstrated the rGPS cycle for 1 hour with a CO_2-fixing rate of 1.36 mM h^{-1} (66.9 nmol min^{-1} mg^{-1} of core cycle proteins, Supplementary Fig. 10f).

Demonstration of the rGPS–MCG cycle. To form a self-replenishing system, we integrated the MCG pathway with the rGPS cycle. The resulting network can produce acetyl-CoA(C_2), pyruvate (C_3) or malate (C_4) directly from CO_2. To confirm the self-replenishing feature, we started the reaction with 0.2 mM of unlabelled crotonyl-CoA and fed the in vitro systems with ^{13}C-labelled bicarbonate and ^{13}C-labelled formate that was converted into $^{13}CO_2$ through Fdh during NADH regeneration. Fully labelled C_2, C_3 and C_4 intermediates will be formed only when the double-labelled glyoxylate enters the MCG cycle as shown in Supplementary Fig. 14. The double-labelled glyoxylate will be formed only when the rGPS cycle runs through at least twice (Supplementary Fig. 15). No triple labelled PEP was produced by rGPS alone (Supplementary Fig. 16a), and double-labelled acetyl-CoA produced by rGPS alone (from the natural abundance of isotopes of C, H, N, O, P and S) was much less than that produced by rGPS–MCG (Supplementary Fig. 16b). Thus, these results proved the intended activity of MCG for the establishment of self-replenishing cycle.

Operation with opto-sensing of cofactor regenerations. To sustain the operation, metabolite and enzyme stability need to be

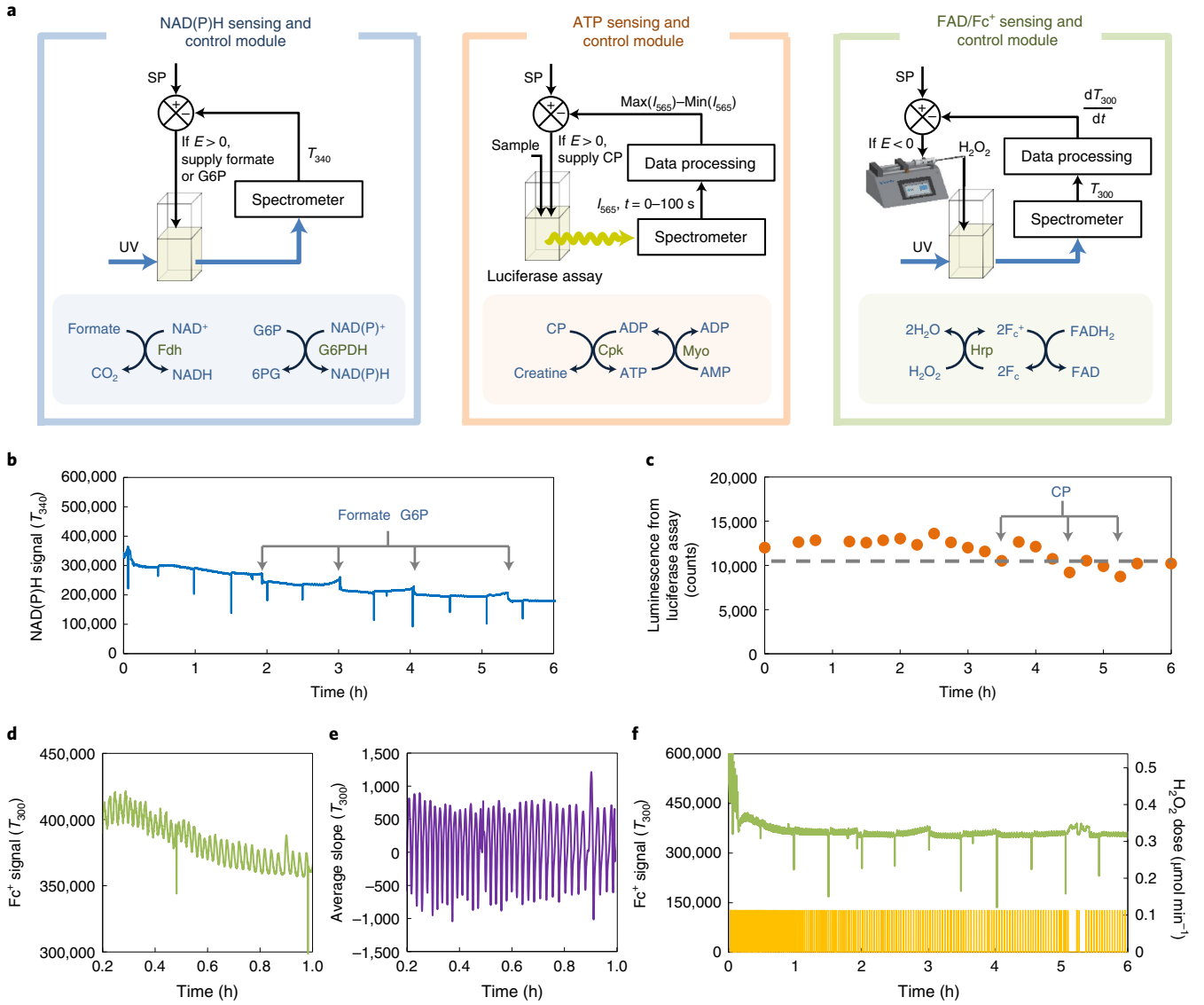

Fig. 2 | Real-time monitoring and control of cofactor regenerations in the rGPS–MCG cycle. a, The cofactor opto-sensing and control modules. **b**, NAD(P)H was monitored by T_{340} over 6 h. Once NAD(P)H was lower than the setpoint (0.3 mM), additional 2.5 mM formate and 0.5 mM G6P were added to the system. **c**, ATP was monitored by the luciferase assay. Assay reagents were mixed with the sample in a cuvette automatically through two Hamilton PSD/4 Precision Syringe Pumps. The bioluminescence from the mixture was measured by a spectrometer. Once ATP was lower than 0.6 mM (10,000 counts), additional 2 mM creatine phosphate (CP) was added to the system. **d**, Dynamics of Fc^+ signal (T_{300}, green line) and the H_2O_2 dose (yellow line) from the feedback-controlled auto-injector over 6 h. **e**, The initial change of Fc^+ signal was due to the CoA compound redistribution. **f**, The average slope of Fc^+ signal at the initial stage. The setpoint of the average slope of T_{300} is 200 within the first hour. Cpk, creatine kinase; Myo, myokinase; Fdh, formate dehydrogenase; G6PDH, glucose-6-phosphate dehydrogenase; Hrp, horseradish peroxidase. G6P, glucose-6-phosphate; 6PG, 6-phosphogluconolactone; Fc, ferrocene; Fc^+, ferrocenium. SP, setpoint; I_{565}, the light intensity at 565 nm; *E*, control error equal to SP-measured output; T_{300}, transmission at 300 nm and T_{340}, transmission at 340 nm. The SP for the NAD(P)H module was set to 0.3 mM, for the ATP module was set to 0.6 mM, and for the FAD/Fc^+ module was set to 200 (counts per second).

addressed. Free CoA is oxidized to CoA disulfide in the presence of oxygen (Supplementary Fig. 17), and the reaction is further promoted by high concentration of H_2O_2 (Supplementary Fig. 18). Additionally, acetyl-CoA binds to some ingredients such as BSA in enzyme preparations. Therefore, all of commercial enzymes were presaturated with acetyl-CoA and column purified. We also found that *E. coli* AtoB is particularly sensitive to H_2O_2 (Supplementary Fig. 19a). Therefore, we replaced AtoB with an isoenzyme, *Rhodobacter sphaeroides* acetyl-CoA acetyltransferase (PhaA), which is relative insensitive to H_2O_2 (Supplementary Fig. 19b). On the other hand, if the H_2O_2 concentration is too low, the FAD regeneration and Mcd activity will be compromised, leading to methylsuccinate formation from the unstable methylsuccinyl-CoA. Fortunately, we found that methylsuccinate can be converted back to methylsuccinyl-CoA through the malate thiokinase (Mtk) in the MCG cycle (Supplementary Fig. 20), although the specific activity of Mtk on methylsuccinate is only about 10% of activity on malate. The formation and conversion of methylsuccinate to methylsuccinyl-CoA form an ATP-draining futile cycle, which should be minimized. As such, H_2O_2 concentration for the FAD regeneration requires precise control to increase the CO_2 fixation efficiency and sustain the cycle.

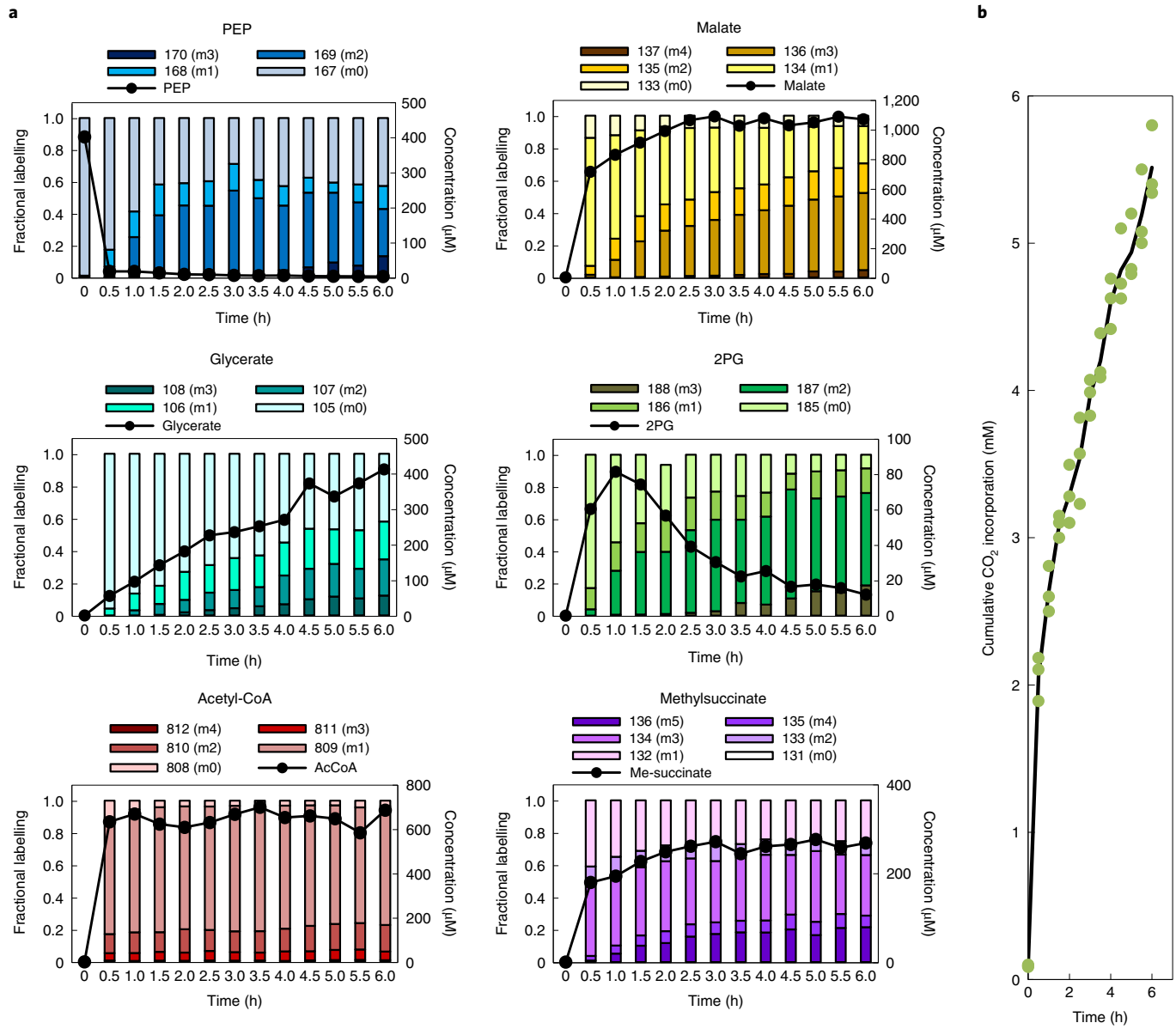

Fig. 3 | The rGPS–MCG cycle with opto-sensing and control module for CO_2 fixation. a, Dynamics of the fractional labelling patterns (on the left *y* axis) and the concentrations (on the right *y* axis) of six major metabolites of the rGPS–MCG cycle over 6 h. These metabolites were measured by LC–MS every 30 min. **b**, The cumulative CO_2 incorporation over 6 h. Cumulative CO_2 incorporation was calculated on the basis of all of the measured labelled carbons among these six intermediates. The data represent the means of $n = 3$ biologically independent experiments.

In addition to the control of FAD regeneration, we identified that NAD(P)H concentration and ATP concentration must also be monitored and controlled. Specifically, we found that Hrp can also oxidize NADH and NADPH with H_2O_2, although the activity is more than 1,000 times lower than its activity with Fc^+ (Supplementary Figs. 11 and 12). It has been known that ATP regulates the enzyme activity through substrate inhibition or allosteric regulation. Here, we identified that high concentration of ATP inhibited the activity of Pps, Mtk and Gk. (Supplementary Figs. 21 and 22b).

In cells, the metabolite concentration and cofactor balance are well-regulated through multiple mechanisms. To substitute for these regulatory circuits, we built a fibre-optic system for automatic real-time monitoring and controlling of the regeneration of NAD(P)H, Fc^+ and ATP as shown in Fig. 2a and Supplementary Fig. 23. To avoid interference from components such as enzymes and CoA-containing metabolites, we extracted 300 ± 5 nm from a deuterium lamp and measured the transmission (T_{300}) for Fc^+ to control the rate for H_2O_2 addition to regenerate FAD. After adjusting for various interfering factors, including a consistent slope decrease due to the initial redistribution of the CoA compound from the starting material (0.4 mM PEP and 0.4 mM crotonyl-CoA) (Fig. 2d,e), we were able to control the H_2O_2 concentration on the basis of the average slope of Fc^+ signal both during the initial phase where the baseline dropped (Fig. 2d–f), and the quasi-steady-state phase where the baseline stabilized. Along the experiment, the signal to noise ratio of the Fc^+ signal decreased, probably due to the limited solubility of ferrocene (Fc) in water, leading to a decrease of the total concentrations of Fc^+ and Fc after repeated reduction and oxidation cycles. This problem can be solved by modifying Fc to increase its solubility. For the NAD(P)H monitoring, we extracted 340 ± 5 nm from the deuterium lamp and measured the transmission (T_{340}). If the T_{340} signal increases more than 7.5%, then the substrates

Table 1 | Comparison of the in vitro carbon fixation results of rGPS-MCG and CETCH 5.4 (ref. [21])

Name	CETCH 5.4	rGPS-MCG
Final product conc. (mM)	0.54 mM glyoxylate	0.7 mM acetyl-CoA 0.4 mM glycerate and 1 mM malate[a]
Starting substrate (mM)	0.2 mM propionyl-CoA	0.4 mM crotonyl-CoA 0.4 mM PEP
Reaction volume (ml)	0.52	20
Core enzyme amounts (μg)[b]	1,196	9,744[c]
Reaction time (h)	1.5	6
Specific CO_2 fixation rate (nmol min^{-1} mg^{-1} core enzyme)	5	100 (0–1.5 h) 28.5 (0–6 h)

[a]Only the major products from the rGPS-MCG cycle were listed [b]Pathway enzymes without enzymes in NAD(P)H, ATP and FAD regeneration system. [c]5,456 μg of enzyme was added initially. 4,288 μg was the total amount of the unstable enzymes that were evenly distributed and added to reaction every 30 min.

(formate and G6P) for NADH and NADPH regeneration were added to the system as shown in Fig. 2b.

The creatine kinase (Cpk) and creatine phosphate system was chosen over the polyphosphate kinase (Ppk) and polyphosphate system for ATP regeneration due to its lower inhibition of ATP-consuming enzymes (Pps, Mtk and Gk) (Supplementary Note 1). ATP concentration was automatically monitored by the luciferase assay every 30 min (Supplementary Fig. 23 and Fig. 2c). To maintain activities and avoid inhibitions of the ATP-consuming enzymes, we set the working concentration of ATP between 0.6 and 0.8 mM. Creatine phosphate, the substrate for ATP regeneration, was added once ATP concentration fell below 0.6 mM (Fig. 2c).

Enzyme limitation. To sustain the CO_2 fixation cycle, we used the principle of pathway assays developed previously[34] and explained in the Methods to identify the limiting enzymes in the system at various times of the reaction. To do so, we divided the rGPS–MCG cycle into four linear segments: acetyl-CoA to ethylmalonyl-CoA; crotonyl-CoA to acetyl-CoA and pyruvate; pyruvate to acetyl-CoA and glyoxylate to PEP (excess amounts of Ppc and Mdh were added for converting PEP to malate to avoid the reversibility of Eno). All enzymes from glyoxylate to PEP were stable (Supplementary Fig. 24). Comparison of the pathway assays results between the initial (Supplementary Fig. 25) and the 6 h enzyme mixture showed that the limiting step shifted along with time, presumably due to enzyme inactivation during the reaction. Among the most unstable enzymes are PhaA, Ccr (Supplementary Fig. 26a), Epi, Ecm, Mcd (Supplementary Fig. 27a), Pps, Ppc, Mtk and Mcl (Supplementary Fig. 28a). We found that PhaA (Supplementary Fig. 26), Ppc, Mtk and Mcl (Supplementary Fig. 28) lost a notable amount of activity after 6 h in the operating conditions, but these enzymes remain stable in the reaction buffer without Fc^+ or H_2O_2. It is likely that protein oxidation by Fc^+ or H_2O_2 caused enzyme instability. On the other hand, the activity of Ccr (Supplementary Fig. 26b) Epi, Ecm, Mcd (Supplementary Fig. 27b) and Pps (Supplementary Fig. 28b) decrease after 6 h incubation even in the reaction buffer in absence of Fc^+ and H_2O_2, suggesting that these enzymes are intrinsically unstable under the ambient condition. To make up for the decreased activities, these unstable enzymes were added to the reaction mixture every 30 min.

After installing the control systems and identifying limiting factors, we achieved a quasi-steady-state operation for the rGPS–MCG cycle for 6 h (Fig. 3). Almost every intermediate in the rGPS–MCG cycle was measured using the liquid chromatography–mass spectrometry (LC–MS) method we established except mesaconyl-C1-CoA, mesaconyl-C_4-CoA and tartronate semialdehyde. We used 0.4 mM of PEP and 0.4 mM crotonyl-CoA to start the reaction. Thus, there was 2.8 mM of unlabelled carbon atom initially. To quantify CO_2 fixation, we fed the in vitro systems with ^{13}C-labelled bicarbonate and ^{13}C-labelled formate that was converted into $^{13}CO_2$ through Fdh during NADH regeneration. Figure 3a shows the time course of concentrations and fractional labelling patterns of six different intermediates in the rGPS–MCG cycle along 6 h operation. As expected, the labelled fraction of every metabolite increased along the reaction. The main carbon reservoir for this CO_2 fixation system was malate, acetyl-CoA and glycerate. 1 mM of malate, 0.7 mM of acetyl-CoA and 0.4 mM of glycerate accumulated within 6 h. At 6 h, about 5% of malate, 12% of glycerate, 13% of PEP and 19% of 2-phospho-D-glycerate were fully labelled, confirming the self-replenishing feature of the rGPS–MCG cycle. Notably, methylsuccinate concentration was maintained below 0.3 mM, indicating that our opto-sensing module for controlling H_2O_2 concentration and FAD regeneration was effective. About 5.5 mM of CO_2 was fixed within 6 h (Fig. 3b). After the initial stage (that is, 1.5 h), a roughly constant CO_2 fixation rate (0.55 mM h^{-1}) and a repeated injection pattern of H_2O_2 dose (Fig. 2d) were achieved, suggesting that the CO_2 fixation system is robust and sustainable within this time frame.

Discussion

To our knowledge, this rGPS–MCG cycle achieved the highest steady-state CO_2 fixation rate (0.55 mM h^{-1}) among complex biocatalytic pathways established fully in vitro. On the basis of the core protein amounts (pathway enzymes without the enzymes in NAD(P)H, ATP and FAD regeneration systems), this rGPS–MCG cycle achieved a higher protein efficiency for CO_2 fixation (28.5 nmol min^{-1} mg^{-1} core cycle protein at quasi-steady state; 100 nmol min^{-1} mg^{-1} core cycle protein within the initial 1.5 h) than the previously reported CETCH 5.4 cycle[21] (Table 1). If we compared our rGPS–MCG cycle with autotrophic and heterotrophic CO_2-fixing microbes on the basis of dry weight, our specific CO_2-fixation rate (28.5 nmol min^{-1} mg^{-1} core protein or 2 mmol h^{-1} g^{-1} core protein) is at least threefold higher than the rate reported in the literature[35] and is comparable to the maximum CO_2 specific uptake rate of *Synechocystis* PCC 6803 during the log phase[36]. Assuming the 50% of dry cell weight is protein, the maximum specific CO_2-fixation rate of *Synechocystis* is about 4 mmol h^{-1} g^{-1} total protein. Alternatively, we can compare the specific CO_2-fixation rate between the rGPS–MCG cycle and the CBB cycle. In *Synechocystis*, approximately 3% of the dry cell weight comes from the CBB cycle[37]. On the basis of these data, the maximum specific CO_2-fixation rate of the CBB cycle in *Synechocystis* is about 65 mmol h^{-1} g^{-1} CBB protein. While this paper was under review, the CBB cycle and rPS pathway were predicted to have pathway activities in the same order of magnitude through the enzyme cost minimization algorithm[23].

The self-replenishing rGPS–MCG cycle designed here enables the production of the key metabolites, such as acetyl-CoA, pyruvate and malate, which can be further converted to almost all chemicals in the biosphere. The cell-free CO_2 fixation system might become practical if these enzymes can be further stabilized and cofactors can be regenerated using renewable energy at a deployable scale and with a sufficiently low cost. Although the enzyme stability remains an issue, this problem can in principle be solved by bioprospecting more stable enzymes or by directed evolution coupled with rational design.

Methods

Materials. All chemicals used were purchased from Sigma-Aldrich unless otherwise specified. Oligonucleotides were purchased from IDT. KOD and KOD

Xtreme DNA polymerase were purchased from EMD Millipore. Gibson Assembly Master Mix was purchased from New England Biolabs.

Culture medium and conditions. *E. coli* strains were grown in Luria-Bertani medium with appropriate antibiotics at 37 °C (for general molecular biology purposes) or 30 °C (for protein expression). Antibiotics were used at the following concentrations: carbenicillin, 200 μg ml^{-1}; spectinomycin, 50 μg ml^{-1} and kanamycin, 50 μg ml^{-1}.

Plasmid construction. All plasmids constructed in this study were assembled using the Gibson isothermal DNA assembly method. pQE9 (Qiagen) or pCDF-Duet1 (Novagen) was used as the plasmid backbone. Plasmids are list in Supplementary Table 4. Primers used are listed in Supplementary Table 5. All plasmids were constructed in *E. coli* strain XL-1 blue for propagation and storage.

Protein purification. *E. coli* strain XL-1 blue or BL21(DE3) was used as host for protein expression. Induction was accomplished with 0.5 mM isopropyl-β-D-thiogalactoside. His-tagged enzymes were purified by cOmplete His-Tag Purification Resin (Sigma-Aldrich). Protein concentrations were determined by the Bradford protein assay using Pierce Coomassie Plus Assay Kit (Thermo Fisher Scientific).

Enzyme assays. See Supplementary Methods for details.

High-performance liquid chromatography analysis. See Supplementary Methods for details.

Conditions for demonstration of the rGPS cycle in two pots. See Supplementary Methods for details.

Conditions for one-pot stepwise reconstitution of the rGPS cycle. See Supplementary Methods for details.

Assay of continuous running of the rGPS cycle using electrochemical FAD regeneration system. See Supplementary Methods for details.

Setup of the electrochemical system. See Supplementary Methods for details.

Assay of continuous running of the rGPS cycle using enzymatic FAD regeneration system. See Supplementary Methods for details.

Building automatic opto-sensing modules for monitoring and controlling cofactor concentrations. To construct a stable monitoring and control system, an all-fibre-based optical system was designed as Supplementary Fig. 23.

For Fc^+ and NAD(P)H monitoring, a ultraviolet light (SLS 204, Thorlabs) was first passed through a colorglass filter (FGUV5M) and was collimated onto the reaction chamber. Then, the transmission intensity at 300 and 340 nm was measured every second by a spectrometer (EE2063S-050-FUVN, Isuzu Optics).

A Luciferase kit was used for ATP measurement. Here, 28 μl of luciferase solution was mixed with 672 μl of water and 20 μl of sample in a cuvette automatically through two Hamilton PSD/4 Precision Syringe Pumps. The bioluminescence from the mixture was measured by a spectrometer (Kymera-328i, Andor) with cooling camera (DU420A-BEX2-DD, Andor) at −70 °C.

All of the optical data were collected through LabVIEW 2020. The pump system for ATP measurement was controlled through a Python v.3.6 code. All of these computer codes are available at https://github.com/gbliao00/CO2_Fix_Machine/tree/master/Paper_relative.

Control algorism for H_2O_2 injection to maintain Fc^+ concentration. To control the H_2O_2 injection while the Fc^+ signal (300 nm) maintained a consistent slope in the first hour due to CoA product distribution, a slope of the linear regression among the most recent 30 points was used to process the transmission signals (counts) at 300 ± 5 nm. The setpoints was set to 200 (counts per s). While rPS pathway was running, the slope increased due to the reduction of Fc^+. If the slope was larger than 200, the syringe pump (LEGATO 100, KD Scientific) was triggered to inject H_2O_2 (250 mM) at the rate of 0.0045 ml min^{-1}. Then, when Fc was oxidized back to Fc^+ by H_2O_2, the slope of signals decreased. The syringe pump was stopped when the slope was lower than 200.

This control algorism was implemented through LabVIEW 2020, which is available at https://github.com/gbliao00/CO2_Fix_Machine/tree/master/Paper_relative.

ATP signal processing. Bioluminescence signals from luciferase assay was measured as a summation of signals from 500 to 700 nm every second using (Kymera-328i, Andor) with cooling camera (DU420A-BEX2-DD, Andor) at −70 °C.

The ATP signal was calculated as $S - B_0$, where the background signal (B_0) was calculated as the median of signals within 12 s before sample injection. The sample signal (S) was calculated as the median of signals within 12 s after sample injection.

The ATP signal from the luciferase assay was calculated by LabVIEW 2020. It is available at https://github.com/gbliao00/CO2_Fix_Machine/tree/master/Paper_relative.

Assays of ATP inhibitions on Mtk, Gk and Pps. For the Mtk assay, the assay was performed in a 600 μl (final volume) reaction mixture containing 100 mM MOPS pH 7.0, 100 mM $NaHCO_3$, 1 mM $MgCl_2$, 1 mM CoA, 0.55 μM FAD, 0.55 μM coenzyme B12, 0.5 mM TPP, 0.5 mM malate, 1 mM creatine phosphate, 4 mM phenylhydrazine, 5 μg of Mtk and 20 μg of Mcl. Reactions were started by adding different concentrations of ATP. Mtk activity was measured by monitoring the increase of absorbance at 324 nm corresponding to the production of glyoxylate-phenylhydrazone.

For the Gk assay, the assay was performed in a 600 μl (final volume) reaction mixture containing 100 mM MOPS pH 7.0, 100 mM $NaHCO_3$, 1 mM $MgCl_2$, 0.3 mM NADH, 1 mM CoA, 0.55 μM FAD, 0.55 μM coenzyme B12, 0.5 mM TPP, 0.5 mM glycerate, 1 mM creatine phosphate, 4 U of Mdh, 2 U of Ppc, 2 U of Eno, 5 U of Cpk and 5 μg of Gk. Reactions were started by adding different concentrations of ATP. Gk activity was measured by monitoring the decrease of absorbance at 340 nm corresponding to the consumption of NADH.

For the Pps assay, the assay was performed in a 600 μl (final volume) reaction mixture containing 100 mM MOPS pH 7.0, 100 mM $NaHCO_3$, 1 mM $MgCl_2$, 0.3 mM NADH, 1 mM CoA, 0.55 μM FAD, 0.55 μM coenzyme B12, 0.5 mM TPP, 0.5 mM pyruvate, 1 mM creatine phosphate, 4 U of Mdh, 2 U of Ppc, 5 U of Cpk and 5 μg of Pps. Reactions were started by adding different concentrations of ATP. Pps activity was measured by monitoring the decrease of absorbance at 340 nm corresponding to the consumption of NADH.

Pathway assays. The principle of pathway assay is to measure the pathway activity by the product of the combined reactions of multiple enzymes. By comparing the pathway activities in the following experiments, one can deduce the possible limiting steps.

(1) Reaction mixture (or cell extract) without supplementing with any enzymes. This serves as a baseline measurement to show that the reaction mixture can perform the desired reaction sequence.
(2) Reaction mixture (or cell extract) supplemented with all enzymes to a given level. This serves as a positive control to show that the pathway activity can be elevated by the addition of all enzymes together.
(3) Reaction mixture (or cell extract) supplemented with all but one enzyme to a given level. If the pathway activity (of experiment 2) is not affected by leaving out this enzyme in the supplement, it suggests that this enzyme is not limiting in the original reaction mixture. On the other hand, if the pathway activity (of experiment 2) is affected by leaving out this enzyme in the supplement, it suggests that this enzyme is limiting.
(4) Repeating experiment 3 by leaving out one enzyme at a time, one can identify all the limiting steps.

On the basis of the principle of pathway assay, the rGPS–MCG cycle was divided into four linear segments: acetyl-CoA to ethylmalonyl-CoA; crotonyl-CoA to acetyl-CoA and pyruvate; pyruvate to acetyl-CoA and glyoxylate to PEP for the pathway assay. All the samples contained the rGPS–MCG enzymes as listed in Supplementary Table 7. These enzyme mixtures were either incubated in the buffer (100 mM HEPES pH 7.2, 100 mM $NaHCO_3$, 1 mM $MgCl_2$, 0.55 μM FAD, 0.55 μM coenzyme B12 and 0.5 mM TPP) or performed in a 6-h operation. The enzyme mixtures were column purified through the Amicon Ultra-0.5 Centrifugal Filter Unit (10 kDa, Merck) four times with the buffer (100 mM HEPES pH 7.2, 100 mM $NaHCO_3$, 1 mM $MgCl_2$, 0.55 μM FAD, 0.55 μM coenzyme B12 and 0.5 mM TPP) to remove the metabolites.

For the assay from acetyl-CoA to ethylmalonyl-CoA, the assay mixture (50 μl) contained 100 mM HEPES pH 7.2, 100 mM $NaHCO_3$, 1 mM $MgCl_2$, 1 mM NADH, 1 mM NADPH, 0.55 μM FAD, 0.55 μM coenzyme B12, 0.5 mM TPP. The initial enzyme amounts from different conditions (initial mixture, 3 and 6 h incubation and 6 h operation), and the additions of fresh enzymes are listed in Supplementary Figs. 25 and 26. Reactions were started by adding 1 mM acetyl-CoA. Ethylmalonyl-CoA was measured by LC–MS.

For the assay from crotonyl-CoA to acetyl-CoA, the assay mixture (70 μl) contained 100 mM HEPES pH 7.2, 100 mM $NaHCO_3$, 1 mM $MgCl_2$, 1 mM NADPH, 0.55 μM FAD, 0.55 μM coenzyme B12, 0.5 mM TPP and 10 μg of Ccr. The initial enzyme amounts from different conditions and the additions of fresh enzymes are listed in Supplementary Figs. 25 and 27. Reactions were started by adding 0.3 mM crotonyl-CoA and 0.35 mM Fc^+. Acetyl-CoA was measured by LC–MS.

For the assay from pyruvate to acetyl-CoA, the assay mixture (50 μl) contained 100 mM HEPES pH 7.2, 100 mM $NaHCO_3$, 1 mM $MgCl_2$, 1 mM NADH, 0.6 mM ATP, 1 mM creatine phosphate, 1 mM CoA, 0.55 μM FAD, 0.55 μM coenzyme B12, 0.5 mM TPP and 0.5 U of Cpk. The initial enzyme amounts from different conditions and the additions of fresh enzymes are listed in Supplementary Figs. 25 and 28. Reactions were started by adding 0.5 mM pyruvate. Acetyl-CoA was measured by LC–MS.

For the assay from glyoxylate to PEP, the assay mixture (50 μl) contained 100 mM HEPES pH 7.2, 100 mM $NaHCO_3$, 1 mM $MgCl_2$, 1 mM NADH, 0.6 mM

ATP, 1 mM creatine phosphate, 0.55 μM FAD, 0.55 μM coenzyme B12, 0.5 mM TPP, 0.5 U of Cpk, 1 U of Ppc and 5 U of Mdh. The initial enzyme amounts from different conditions and the additions of fresh enzymes are listed in Supplementary Figs. 24 and 25. Reactions were started by adding 1 mM glyoxylate. Malate was measured by LC–MS.

Assay of 6 h operation of the rGPS–MCG cycle using enzymatic FAD regeneration system. The reaction mixture (20 ml as the final volume) contained 100 mM HEPES pH 7.2, 100 mM $NaH^{13}CO_3$, 1 mM $MgCl_2$, 0.15 mM NADH, 0.1 mM NAD^+, 0.15 mM NADPH, 0.8 mM ATP, 5 mM ^{13}C sodium formate, 1 mM glucose-6-phosphate, 5 mM creatine phosphate, 40 μg ml^{-1} gentamycin (for preventing bacteria contamination, see Supplementary Note 2), 0.18 mM CoA, 0.55 μM FAD, 0.55 μM coenzyme B12, 0.5 mM TPP and 0.12 mM $FePF_6$ (Fc^+), and all the enzymes with the corresponding amounts (Supplementary Table 7). All the commercial enzymes (Myo, Hrp, Zwf, Cpk, Ppc, Mdh and Eno) were column purified through the Amicon Ultra-0.5 Centrifugal Filter Unit (10 kDa, Merck) with 100 mM HEPES buffer containing 1 mM $MgCl_2$, 0.55 μM FAD, 0.55 μM coenzyme B12, 0.5 mM TPP and 0.5 mM acetyl-CoA. The unstable enzymes (Supplementary Table 7) were added into the reaction mixture every 30 min. The reaction was initiated with the addition of 0.4 mM PEP and 0.4 mM crotonyl-CoA.

Fc^+ and NAD(P)H concentration was monitored through the transmission at 300 ± 5 and 340 ± 5 nm, respectively. Fc^+ concentration was controlled through an automatic syringe pump as mentioned before. The setpoint of NAD(P)H total concentration was 0.3 mM. Once NAD(P)H concentration was lower than the setpoint, 2.5 mM ^{13}C sodium formate and 0.5 mM G6P were added into the reaction mixture. ATP concentration was measured through luciferase assay automatically as mentioned before. The setpoint of ATP concentration was 0.6 mM. Once ATP concentration was lower than the setpoint, 2.5 mM creatine phosphate was added into the reaction mixture. Metabolite concentrations and their labelling patterns were measured through LC–MS (LC–MS-8045, Shimadzu) every 30 min.

LC–tandem MS (LC–MS/MS) analysis. Metabolite concentrations and their labelling patterns were measured and analysed by triple quadrupole Shimadzu LC–MS 8045 with YMC-Triart C18 ExRS (Metal free column) (150 × 2.1 mm^2, 1.9 μm, product no. TAR08SP9-15Q1PTP) at a flow rate of 0.30 ml min^{-1}. Separation was performed using a gradient system of 100 mM tributylamine and 150 mM acetic acid with 0.4 mM NH_4F (solvent A) and 100% methanol and 0.4 mM NH_4F (solvent B). At the start was 95% solvent A and 5% solvent B. Solvent B was increased linearly to 25% over 4 min after starting point. From 4 to 10 min, solvent B was increased to 98% linearly and was maintained at 98% for 10.2 min. At 20.2 min, solvent B was decreased to its initial 5% within 0.5 min and held for 4.8 min to reequilibrate the column. The column temperature was maintained at 50 °C and the injection volume was 2 μl. LC–MS/MS was set in the negative mode with spectra acquired over a mass range of 50–1,000 *m/z*. The acquisition parameters were as follows: interface temperature, 250 °C; desolvation line temperature, 200 °C; heat block temperature, 400 °C; desolvation gas, nitrogen; nebulizing gas flow rate, 3.0 l min^{-1}; drying gas, nitrogen and drying gas flow rate, 5 l min^{-1}. All of the metabolites and their labelling patterns were measured by multiple reaction monitoring (MRM (−)).

Pathway thermodynamics analysis. Maximum–minimum driving force analysis[27] was applied to evaluate the thermodynamics feasibility of the pathway. Python packages equilibrator_api (v.0.4.5) and equilibrator_pathway (v.0.4.5) were used for the analysis. The change in Gibbs energy of the reactions was estimated using the component contribution method[28]. CO_2 was considered as the substrate for the carboxylation reactions as its concentration is pH-independent, unlike that of bicarbonate, thus simplifying the calculations. Metabolite concentrations were constrained to the range of 1 μM to 10 mM as described previously[27]. pH was assumed to be 7.0, ionic strength was assumed to be 0.25 M and $-\log[Mg^{2+}]$ (pMg) was assumed to be 3.

Reporting Summary. Further information on research design is available in the Nature Research Reporting Summary linked to this article.

Data availability

The data that support the plots within this paper and other findings of this study are available from the corresponding author on reasonable request.

Code availability

All of the optical data were collected through LabVIEW 2020. The pump system for ATP measurement was controlled through a Python 3.6 code. The ATP signal from the luciferase assay was calculated by LabVIEW 2020. All of these computer codes are available at https://github.com/gbliao00/CO2_Fix_Machine/tree/master/Paper_relative.

Received: 3 July 2021; Accepted: 13 January 2022;
Published online: 24 February 2022

References

1. Friedlingstein, P. et al. Global carbon budget 2020. *Earth Syst. Sci. Data* **12**, 3269–3340 (2020).
2. Guterres, A. United Nations Secretary-General. *Carbon Neutrality by 2050: The World's Most Urgent Mission* (United Nations, 2020); https://www.un.org/sg/en/content/sg/articles/2020-12-11/carbon-neutrality-2050-the-world%E2%80%99s-most-urgent-mission
3. Magliery, T. J. Protein stability: computation, sequence statistics, and new experimental methods. *Curr. Opin. Struct. Biol.* **33**, 161–168 (2015).
4. Chandler, P. G. et al. in *Protein Nanotechnology: Protocols, Instrumentation, and Applications* 163–181 (Methods in Molecular Biology series no. 300) (Springer, 2005).
5. Lerma-Ortiz, C. et al. 'Nothing of chemistry disappears in biology': the top 30 damage-prone endogenous metabolites. *Biochem. Soc. Trans.* **44**, 961–971 (2016).
6. Wagner, G. R. et al. A class of reactive acyl-CoA species reveals the non-enzymatic origins of protein acylation. *Cell. Metab.* **25**, 823–837.e8 (2017).
7. Shi, T., Han, P., You, C. & Zhang, Y.-H. P. J. An in vitro synthetic biology platform for emerging industrial biomanufacturing: bottom-up pathway design. *Synth. Syst. Biotechnol.* **3**, 186–195 (2018).
8. Barenholz, U. et al. Design principles of autocatalytic cycles constrain enzyme kinetics and force low substrate saturation at flux branch points. *eLife* **6**, e20667 (2017).
9. Braakman, R. & Smith, E. The emergence and early evolution of biological carbon-fixation. *PLoS Comput. Biol.* **8**, e1002455 (2012).
10. Sánchez-Andrea, I. et al. The reductive glycine pathway allows autotrophic growth of *Desulfovibrio desulfuricans*. *Nat. Commun.* **11**, 5090 (2020).
11. Fuchs, G. Alternative pathways of carbon dioxide fixation: insights into the early evolution of life? *Annu. Rev. Microbiol.* **65**, 631–658 (2011).
12. Ganti, T., Szathmary, E. & Griesemer, J. *The Principles of Life* (Oxford Univ. Press, 2003).
13. Erb, T. J. Carboxylases in natural and synthetic microbial pathways. *Appl. Environ. Microbiol.* **77**, 8466–8477 (2011).
14. Erb, T. J. & Zarzycki, J. A short history of RubisCO: the rise and fall (?) of nature's predominant CO_2 fixing 2 enzyme. *Curr. Opin. Biotechnol.* **49**, 100–107 (2018).
15. Chabrière, E. et al. Crystal structures of the key anaerobic enzyme pyruvate:ferredoxin oxidoreductase, free and in complex with pyruvate. *Nat. Struct. Mol. Biol.* **6**, 182–190 (1999).
16. Izui, K., Matsumura, H., Furumoto, T. & Kai, Y. Phosphoenolpyruvate carboxylase: a new era of structural biology. *Annu. Rev. Plant Biol.* **55**, 69–84 (2004).
17. Bar-Even, A., Noor, E., Lewis, N. E. & Milo, R. Design and analysis of synthetic carbon fixation pathways. *Proc. Natl Acad. Sci. USA* **107**, 8889–8894 (2010).
18. Mainguet, S. E., Gronenberg, L. S., Wong, S. S. & Liao, J. C. A reverse glyoxylate shunt to build a non-native route from C4 to C2 in *Escherichia coli*. *Metab. Eng.* **19**, 116–127 (2013).
19. Yu, H., Li, X., Duchoud, F., Chuang, D. S. & Liao, J. C. Augmenting the Calvin–Benson–Bassham cycle by a synthetic malyl-CoA-glycerate carbon fixation pathway. *Nat. Commun.* **9**, 2008 (2018).
20. Erb, T. J. et al. Synthesis of C5-dicarboxylic acids from C2-units involving crotonyl-CoA carboxylase/reductase: the ethylmalonyl-CoA pathway. *Proc. Natl Acad. Sci. USA* **104**, 10631–10636 (2007).
21. Schwander, T., Schada von Borzyskowski, L., Burgener, S., Cortina, N. S. & Erb, T. J. A synthetic pathway for the fixation of carbon dioxide in vitro. *Science* **354**, 900–904 (2016).
22. Zarzycki, J., Brecht, V., Müller, M. & Fuchs, G. Identifying the missing steps of the autotrophic 3-hydroxypropionate CO_2 fixation cycle in *Chloroflexus aurantiacus*. *Proc. Natl Acad. Sci. USA* **106**, 21317–21322 (2009).
23. Löwe, H. & Kremling, A. In-depth computational analysis of natural and artificial carbon fixation pathways. *Bio-Des. Manuf.* https://doi.org/10.34133/2021/9898316 (2021).
24. Buckel, W. & Thauer, R. K. Energy conservation via electron bifurcating ferredoxin reduction and proton/Na^+ translocating ferredoxin oxidation. *Biochim. Biophys. Acta - Bioenerg.* **1827**, 94–113 (2013).
25. Lenn, N. D., Stankovich, M. T. & Liu, H. W. Regulation of the redox potential of general acyl-CoA dehydrogenase by substrate binding. *Biochemistry* **29**, 3709–3715 (1990).
26. Buckel, W. & Thauer, R. K. Flavin-based electron bifurcation, ferredoxin, flavodoxin, and anaerobic respiration with protons (Ech) or NAD^+ (Rnf) as electron acceptors: a historical review. *Front. Microbiol.* **9**, 401 (2018).
27. Noor, E. et al. Pathway thermodynamics highlights kinetic obstacles in central metabolism. *PLoS Comput. Biol.* **10**, e1003483 (2014).
28. Noor, E., Haraldsdóttir, H. S., Milo, R. & Fleming, R. M. T. Consistent estimation of Gibbs energy using component contributions. *PLoS Comput. Biol.* **9**, e1003098 (2013).

29. Shen, C. R. et al. Driving forces enable high-titer anaerobic 1-butanol synthesis in *Escherichia coli*. *Appl. Environ. Microbiol.* **77**, 2905–2915 (2011).
30. Kortmann, M., Baumgart, M. & Bott, M. Pyruvate carboxylase from *Corynebacterium glutamicum*: purification and characterization. *Appl. Microbiol. Biotechnol.* **103**, 6571–6580 (2019).
31. Berman, K. M. & Cohn, M. Phosphoenolpyruvate synthetase of *Escherichia coli*. Purification, some properties, and the role of divalent metal ions. *J. Biol. Chem.* **245**, 5309–5318 (1970).
32. Kai, Y. et al. Three-dimensional structure of phosphoenolpyruvate carboxylase: a proposed mechanism for allosteric inhibition. *Proc. Natl Acad. Sci. USA* **96**, 823–828 (1999).
33. Inkpen, M. S. et al. Non-chemisorbed gold–sulfur binding prevails in self-assembled monolayers. *Nat. Chem.* **11**, 351–358 (2019).
34. Lin, P. P. et al. Construction and evolution of an *Escherichia coli* strain relying on nonoxidative glycolysis for sugar catabolism. *Proc. Natl Acad. Sci. USA* **115**, 3538–3546 (2018).
35. Gong, F. et al. Quantitative analysis of an engineered CO_2-fixing *Escherichia coli* reveals great potential of heterotrophic CO_2 fixation. *Biotechnol. Biofuels* **8**, 86 (2015).
36. Shabestary, K. et al. Targeted repression of essential genes to arrest growth and increase carbon partitioning and biofuel titers in *Cyanobacteria*. *ACS Synth. Biol.* **7**, 1669–1675 (2018).
37. Jahn, M. et al. Growth of *Cyanobacteria* is constrained by the abundance of light and carbon assimilation proteins. *Cell Rep.* **25**, 478–486.e8 (2018).

Acknowledgements

This work was supported by Sustainability Science Research Program from Academia Sinica (grant nos. AS-SS-109-07 and AS-SS-110-03). We thank S. Sheng-Fa Yu, M. Ming-Hsi Chiang, T. Natarajan, J. Yu-Chiao Liu and K.-T. Chu for scientific discussions. We thank M.-C. Tseng from Institute of Chemistry, Academia Sinica, for helping with identifying the low solubility problem of Fc. We thank S.-Y. Lin and Y.-Y. Chen from the Common Mass Spectrometry Facilities (Academia Sinica) for the discussions about protein stability and modification. We thank H. Yu for solving the expression problem of Mtk. We thank H.-W. Jung, D.N. Streuli, Y.-C. Chiang, J.-Y. Huang, Y.-T. Lai, H. Sebastian and I.C. Lam for helping with protein purifications. We thank B. Wang for helping with the electrochemistry system at UCLA.

Author contributions

J.C.L. designed the rGS and MCG pathways. S.L. designed the rPS pathway. P.P.L., G.-B.L., P.-W.T. and C.C. designed and built the automatic auto-sensing system. S.L. designed and performed the most experiments and analysed the rGPS data. P.P.L. designed the most experiments and analysed the rGPS–MCG data. L.-Y.N. contributed to the design and analysis of pathway assay, methylsuccinyl-CoA regeneration and cofactor regeneration system. P.P.L., L.-Y.N., G.-B.L. and P.W.T. performed the experiments of rGPS–MCG. S.L., P.P.L. and J.C.L. wrote the paper. P.P.L. and J.C.L. edited the paper.

Competing interests

The authors declare no competing interests.

Additional information

Supplementary information The online version contains supplementary material available at https://doi.org/10.1038/s41929-022-00746-x.

Correspondence and requests for materials should be addressed to James C. Liao.

Peer review information *Nature Catalysis* thanks Steffen N. Lindner and the other, anonymous, reviewer(s) for their contribution to the peer review of this work.

Reprints and permissions information is available at www.nature.com/reprints.

Publisher's note Springer Nature remains neutral with regard to jurisdictional claims in published maps and institutional affiliations.

nature portfolio

Corresponding author(s): James C. Liao

Last updated by author(s): Dec 12, 2021

Reporting Summary

Nature Portfolio wishes to improve the reproducibility of the work that we publish. This form provides structure for consistency and transparency in reporting. For further information on Nature Portfolio policies, see our Editorial Policies and the Editorial Policy Checklist.

Statistics

For all statistical analyses, confirm that the following items are present in the figure legend, table legend, main text, or Methods section.

n/a	Confirmed
☐	☒ The exact sample size (*n*) for each experimental group/condition, given as a discrete number and unit of measurement
☐	☒ A statement on whether measurements were taken from distinct samples or whether the same sample was measured repeatedly
☒	☐ The statistical test(s) used AND whether they are one- or two-sided *Only common tests should be described solely by name; describe more complex techniques in the Methods section.*
☒	☐ A description of all covariates tested
☒	☐ A description of any assumptions or corrections, such as tests of normality and adjustment for multiple comparisons
☐	☒ A full description of the statistical parameters including central tendency (e.g. means) or other basic estimates (e.g. regression coefficient) AND variation (e.g. standard deviation) or associated estimates of uncertainty (e.g. confidence intervals)
☒	☐ For null hypothesis testing, the test statistic (e.g. *F*, *t*, *r*) with confidence intervals, effect sizes, degrees of freedom and *P* value noted *Give P values as exact values whenever suitable.*
☒	☐ For Bayesian analysis, information on the choice of priors and Markov chain Monte Carlo settings
☒	☐ For hierarchical and complex designs, identification of the appropriate level for tests and full reporting of outcomes
☒	☐ Estimates of effect sizes (e.g. Cohen's *d*, Pearson's *r*), indicating how they were calculated

Our web collection on statistics for biologists contains articles on many of the points above.

Software and code

Policy information about availability of computer code

Data collection	For the enzyme assays, data were collected by Agilent Cary 3500 UV-Vis Spectrophotometer. For the transmission of Fc and NAD(P)H, data were collected by a spectrometer (EE2063S-050-FUVN, ISUZU OPTICS, Taiwan). For ATP signal from the luciferase assay were collected by a spectrometer (Kymera-328i, Andor) with cooling camera (DU420A-BEX2-DD, Andor) at -70 °C. All of these optical data were collected through LabVIEW 2020 (available at https://github.com/gbliao00/CO2_Fix_Machine/tree/master/Paper_relative). Metabolite concentration data were collected by triple quadrupole Shimadzu LC-MS 8045 with YMC- Triart C18 ExRS [Metal free column].
Data analysis	Data were analyzed by Microsoft Excel 2019, Agilent Cary UV Workstation software and Shimadzu LabSolution PostRun Analysis. The ATP signal from the luciferase assay was calculated by LabVIEW 2020. It is available at https://github.com/gbliao00/CO2_Fix_Machine/tree/master/Paper_relative

For manuscripts utilizing custom algorithms or software that are central to the research but not yet described in published literature, software must be made available to editors and reviewers. We strongly encourage code deposition in a community repository (e.g. GitHub). See the Nature Portfolio guidelines for submitting code & software for further information.

Data

Policy information about availability of data

All manuscripts must include a data availability statement. This statement should provide the following information, where applicable:

- Accession codes, unique identifiers, or web links for publicly available datasets
- A description of any restrictions on data availability
- For clinical datasets or third party data, please ensure that the statement adheres to our policy

The data that support the plots within this paper and other findings of this study are available from the corresponding author upon reasonable request.
All of the computer code in this work are available at https://github.com/gbliao00/CO2_Fix_Machine/tree/master/Paper_relative

Field-specific reporting

Please select the one below that is the best fit for your research. If you are not sure, read the appropriate sections before making your selection.

☒ Life sciences ☐ Behavioural & social sciences ☐ Ecological, evolutionary & environmental sciences

For a reference copy of the document with all sections, see nature.com/documents/nr-reporting-summary-flat.pdf

Life sciences study design

All studies must disclose on these points even when the disclosure is negative.

Sample size	No statistical methods were used to predetermine the sample size. At least three independent experiments were performed in this work. Sample sizes were determined on the basis of previous experiments by considering biological and technical variabilities.
Data exclusions	No data were excluded in this work.
Replication	At least three independent experiments were performed to verify our results. All of the attempts were successful.
Randomization	Randomization was not applicable for the experiments performed, since no statistical comparisons were performed
Blinding	Blinding was not relevant to our study, since no statistical comparisons were performed

Reporting for specific materials, systems and methods

We require information from authors about some types of materials, experimental systems and methods used in many studies. Here, indicate whether each material, system or method listed is relevant to your study. If you are not sure if a list item applies to your research, read the appropriate section before selecting a response.

Materials & experimental systems

n/a	Involved in the study
☒	☐ Antibodies
☒	☐ Eukaryotic cell lines
☒	☐ Palaeontology and archaeology
☒	☐ Animals and other organisms
☒	☐ Human research participants
☒	☐ Clinical data
☒	☐ Dual use research of concern

Methods

n/a	Involved in the study
☒	☐ ChIP-seq
☒	☐ Flow cytometry
☒	☐ MRI-based neuroimaging